

The Nonlinear Evolution of Galaxy Intrinsic Alignments

Jounghun Lee

*Department of Physics and Astronomy, FPRD, Seoul National University, Seoul 151-747,
Korea*

jounghun@astro.snu.ac.kr

Ue-Li Pen

Canadian Institute for Theoretical Astrophysics, Toronto, ON M5S 3H8, Canada

pen@cita.utoronto.ca

ABSTRACT

The non-Gaussian contribution to the intrinsic halo spin alignments is analytically modeled and numerically detected. Assuming that the growth of non-Gaussianity in the density fluctuations caused the tidal field to have nonlinear-order effect on the orientations of the halo angular momentum, we model the intrinsic halo spin alignments as a linear scaling of the density correlations on large scales, which is different from the previous quadratic-scaling model based on the linear tidal torque theory. Then, we analyze the halo catalogs from the recent high-resolution Millennium Run simulation at four different redshifts ($z = 0, 0.5, 1$ and 2) and measure quantitatively the degree of the nonlinear effect on the halo spin alignments and its changes with redshifts. A clear signal of spin correlations is found on scales as large as $10h^{-1}\text{Mpc}$ at $z = 0$, which marks a detection of the nonlinear tidal effect on the intrinsic halo alignments. We also investigate how the nonlinear effect depends on the intrinsic properties of the halos. It is found that the degree of the nonlinear tidal effect increases as the halo mass scale decreases, the halo specific angular momentum increases, and the halo peculiar velocity decreases. We discuss implication of our result on the weak gravitational lensing.

Subject headings: cosmology:theory — large-scale structure of universe

1. INTRODUCTION

The intrinsic galaxy alignment refers to a cosmic phenomenon that the orientations of the galaxy spin axes (or galaxy ellipticities) are not random but locally aligned between neighbors due to the spatial correlations of the initial tidal field. The topic of the intrinsic galaxy alignments has recently drawn considerable attention in the field of the large-scale structure for three reasons. Firstly, since it is believed to be induced by the spatial correlations of the initial tidal field, it will be possible in principle by measuring the galaxy intrinsic alignments to reconstruct the initial density field on galactic scales (Lee & Pen 2000, 2001, 2002; Lee & Erdogdu 2007).

Secondly, the initial tidal correlations are also responsible for the web-like distribution of the large scale structures (Bond, Kofman, & Pogosyan 1996). Thus, the galaxy intrinsic alignments will be useful to characterize and quantify the influence of the large-scale structures on the orientations of the galaxies distributed in a cosmic web (Navarro et. al. 2004; Trujillo et. al. 2006; Patiri et al. 2006; Aragon-Calvo et al. 2007; Hahn et al. 2007).

Thirdly and most importantly, the galaxy intrinsic alignments could cause non-negligible contamination on weak lensing signals. Plenty of efforts have been made so far to distinguish and separate the intrinsic contaminations from the galaxy extrinsic alignments caused by the weak gravitational lensing effect (Croft & Metzler 2000; Heavens et al. 2000; Catelan et al. 2001; Crittenden et al. 2001; Jing 2002; Hui & Zhang 2002; Heymans & Heavens 2003; Takada & White 2004; Hirata & Seljak 2004; King 2005; Mandelbaum et al. 2006).

For these reasons, it is of fundamental importance to predict the degree of galaxy intrinsic alignments with a valid theory and measure quantitatively their signals in practice. In fact, Pen et al. (2000) have provided an analytic model for the intrinsic galaxy spin alignments in the frame of the linear tidal torque theory (Doroshkevich 1970; White 1984; Catelan & Theuns 1996). According to their model, the galaxy intrinsic alignments can be expressed in terms of a quadratic scaling of the density correlation function and thus are expected to exist only at small distances of order of a few Mpc. A crucial implication of their analytic model is that due to the quadratic scaling nature of the galaxy intrinsic alignments the cross-correlations between the gravitational lensing shears from large scale density field and the galaxy intrinsic alignments with local tidal shears will be zero.

Pen et al. (2000) tested their analytic predictions against low-redshift samples of spiral galaxies and found that the observed signals are consistent with the analytic predictions. Yet, their detections suffered from poor-number statistics and thus were still tentative. Later, several other authors have confirmed the existence of galaxy intrinsic alignments at small scales either in numerical simulations or in low-redshift observational surveys (Heavens et al.

2000; Jing 2002; Brown et al. 2002; Heymans et al. 2004).

However, Hui & Zhang (2002) has pointed out that it might be invalid to describe the galaxy intrinsic alignments on large scales as a quadratic function of the density correlation. Their logic is as follows: Since the quadratic scaling is based on the linear tidal torque theory which adopts a somewhat oversimplified assumption that the tidal field is Gaussian in the subsequent evolutionary stages, it should not be a good approximation to describe the galaxy intrinsic alignments on large scales. In reality, the density fluctuations will develop non-Gaussianity via gravity which would in turn lead to non-negligible contributions of the nonlinear-order of the tidal tensors to the generation of the galaxy angular momentum. Due to this nonlinear effect on the galaxy angular momentum, their intrinsic spin alignments should be better approximated as linear scaling with the density correlation function. Because the linear scaling of the density correlation drops much slowly than the quadratic scaling, the intrinsic spin alignments would not be completely negligible even on large scales. If their claims turn out to be true, then it will have a significant impact not only on the weak lensing analysis but also on our fundamental understanding of the evolution of the tidal alignments.

In the light of their claims, the following questions naturally arise; Does the nonlinear tidal effect on the galaxy intrinsic alignments really exist to a non negligible degree? If so, at what epochs and on which scales does its contribution begin to be significant? Does it depend on the intrinsic properties of the galaxies or dark halos? Our goal here is to answer the above questions using both analytical and numerical methods.

The outline of this paper is as follows: §2, we overview briefly the previous analytic model for the galaxy spin-spin alignments based on the linear tidal torque theory and propose a new model to account for the nonlinear tidal effect. §3, we report a detection of the signals of the nonlinear tidal effect on the intrinsic spin alignments of dark matter halos simulated in N-body experiments and show how the signals depend on redshift, scale, and the halo intrinsic property. §4, we summarize our results and discuss the implications of our work on the weak lensing effect.

2. ANALYTIC MODEL

2.1. Overview of the Linear Tidal Torque Theory

The linear tidal torque theory explains that unless a proto-halo has a perfectly spherical shape, it can acquire spin angular momentum at first order through its tidal interaction with the surrounding matter (Doroshkevich 1970; White 1984; Catelan & Theuns 1996). The

main prediction of the linear tidal torque theory is that the proto-halo angular momentum vector, (J_i) , is proportional to the anti-symmetric product of the two tensors, the inertial momentum tensor (I_{ij}) and the local tidal shear tensor, (T_{ij}) , as

$$L_i \propto \epsilon_{ijk} T_{jl} I_{lk}. \quad (1)$$

Here the definitions of I_{ij} and T_{ij} are given as

$$I_{ij} \equiv \int_V d^3 \mathbf{q} \rho(\mathbf{q}) q_i q_j, \quad T_{ij} \equiv \frac{\partial^2}{\partial q_i \partial q_j} \Phi(\mathbf{q}). \quad (2)$$

where \mathbf{q} is the Lagrangian position of the particles that reside in the proto-halo regions, V and $\rho(\mathbf{q})$ are the Lagrangian volume and the density of the proto-halo region, respectively, and $\Phi(\mathbf{q})$ is the velocity perturbation potential.

Given the property of the perfectly anti-symmetric tensor ϵ_{ijk} in equation (1), an additional condition has to be satisfied for the first-order generation of the proto-halo angular momentum: the principal axes of I_{ij} and T_{ij} have to be misaligned with each other (Catelan & Theuns 1996). Furthermore, a crucial implication of equation (1) is that if this additional condition is satisfied and thus the angular momentum of a proto-halo is generated at first order, then the direction of the proto-halo angular momentum is not random but preferentially aligned with the principal axes of the local tidal tensor (Lee & Pen 2000).

Numerical experiments have revealed that the principal axes of (I_{ij}) and (T_{ij}) are correlated strongly but not perfectly (Lee & Pen 2000; Porciani et al. 2002), which indicates that the first-order generation of the proto-halo angular momentum is not so efficient and the degree of the alignments between the proto-halo spin directions and the principal axes of the local tidal shear tensors would not be so high.

Motivated by this numerical clue, Lee & Pen (2000) suggested the following quadratic formula to quantify the expected degree of the alignments between the halo spins and the local tidal shears, generalizing the linear tidal torque theory:

$$\langle \hat{L}_i \hat{L}_j \rangle = \frac{1+a}{3} \delta_{ij} - a \hat{T}_{ik} \hat{T}_{kj}. \quad (3)$$

where (\hat{L}_i) is the unit spin vector of a halo, (\hat{T}_{ij}) is the unit traceless tidal tensor smoothed on the halo mass scale, and a is a correlation parameter in the range of $[0, 3/5]$ which measures the strength of the correlation between (\hat{L}_i) and (\hat{T}_{ij}) . It is worth recalling the fact that the ensemble average $\langle \hat{L}_i \hat{L}_j \rangle$ in the left hand side of equation (3) is obtained by taking the average of $\hat{L}_i \hat{L}_j$ from the sample halos having all different mass, while the tidal shear field in the right hand side of equation (3) is smoothed on the single mass scale which amounts to

the mean halo mass (i.e., the mean value of the mass of the sample halos). Lee & Pen (2000) derived equation (3) empirically, relating the angular momenta of the halos with different mass to the tidal shear field smoothed on the mean halo mass.

The correlation parameter a in equation (3) which characterizes equation (3) is introduced to take into account strong correlations between (I_{ij}) and (T_{ij}) and any modification in the subsequent evolution after the moment of the turn-around. The two extreme cases of $a = 0$ and $a = 3/5$ represent no correlation and maximum correlation between (\hat{L}_i) and (\hat{T}_{ij}) , respectively. It is expected that the true value of a would be between these two extremes.

The linear tidal torque theory itself cannot make any prediction on the value of a . Thus, the true value of this free parameter a has to be determined empirically. So far, several attempts have been made to measure the value of a either from numerical simulations or from observations (Lee & Pen 2000; Porciani et al. 2002; Navarro et. al. 2004; Trujillo et. al. 2006; Lee & Erdogdu 2007). Although no general consensus has been reached on the true value of a , most of the numerical and observational evidences indicated that the true value of a deviates from zero.

2.2. The First Order Approximation to the Halo Spin Correlations

A difficulty in constraining the value of a lies in the fact that it is hard to measure the principal axes of the linear tidal field in real space. An alternative approach to the true value of a is to measure the intrinsic spin-spin correlations of dark halos (Pen et al. 2000). The local alignments between the halo spin vectors and the tidal shear tensors will lead to spatial spin alignments between the neighbor halos. Using equation (3), Pen et al. (2000) derived the following analytic model for the halo spin-spin correlations:

$$\eta(r) \equiv \langle |\hat{\mathbf{J}}(\mathbf{x}) \cdot \hat{\mathbf{J}}(\mathbf{x} + \mathbf{r})|^2 \rangle - \frac{1}{3} \approx \frac{a^2 \xi^2(r; R)}{6 \xi^2(0; R)}. \quad (4)$$

Here, the constant $1/3$ represents the value of $\langle |\hat{\mathbf{J}}(\mathbf{x}) \cdot \hat{\mathbf{J}}(\mathbf{x} + \mathbf{r})|^2 \rangle$ for the case of no alignment, and $\xi(r; R)$ is the linear two-point correlation function defined as

$$\xi(r; R) \equiv \int_{-\infty}^{\infty} \Delta^2(k) \frac{\sin kr}{kr} W^2(kR) d \ln k, \quad (5)$$

where $\Delta^2(k)$ is the dimensionless power spectrum and $W(kR)$ is the top-hat spherical filter of scale radius, R , which is related to the halo mass scale M as $R \equiv [3M/(4\pi\bar{\rho})]^{1/3}$ with the mean density $\bar{\rho}$.

Note that equation (4) is proportional to the square of the two point density correlation $\xi(r)$, which means that the halo spin-spin correlations would decrease very rapidly. For instance, on a galactic scale ($R \sim 1h^{-1}\text{Mpc}$), it is expected that the halo spin-spin correlations exist only at distances of order of a few Mpc and effectively vanishes at larger distances.

Since the tidal field on different scales are cross-correlated, equation (3) leads to the existence of the cross-correlations of the spin axes of halos on different mass scales. In accordance with equation (4) the halo spin cross-correlations on different scales (R_1 and R_2) are modeled as

$$\eta_C(r) \approx \frac{a^2 \xi_C^2(r; R_1, R_2)}{6 \xi_C^2(0; R_1, R_2)}. \quad (6)$$

where $\xi_C^2(r; R_1, R_2)$ is the density cross-correlation function defined as

$$\xi_C(r; R_1, R_2) \equiv \int_{-\infty}^{\infty} \Delta^2(k) \frac{\sin kr}{kr} W(kR_1)W(kR_2) d \ln k. \quad (7)$$

It is worth mentioning that the value of a for the cross correlation $\eta_C(r)$ would not be same as its value for the auto-correlation $\eta(r)$ in equation (4) due to the difference in the smoothing scale for the tidal field. Note that equation (6) is a modified version of equation (4), both of which are based on equation (3). The correlation parameter a in equation (4) represents the spin-spin correlations caused by the spatial correlations of the tidal fields smoothed on the same scale (one mean halo mass scale, R). While the correlation parameter a in equation (6) represents the spin-spin correlations caused by the spatial correlations of the tidal fields on two different scales (two mean halo mass scales, R_1 and R_2). Since the spatial correlations of the two tidal fields smoothed on two different scales, R_1 and R_2 (say, $R_1 < R_2$), are lower than the case that the two tidal fields are smoothed on the same scale of R_2 and higher than the case that they are smoothed on the same scale of R_1 , it is naturally expected that the value of a for the cross-correlation $\eta_C(r)$ should be different from that for the correlation $\eta(r)$.

2.3. The Nonlinear Effect and Large Scale Correlations of Halo Spins

As mentioned in §1, it was Hui & Zhang (2002) who first pointed out that equation (4) is valid only if the gravitational tidal field is Gaussian. They argued that the non-Gaussianity in the tidal field should not be negligible in the nonlinear regime and suggested that the halo spin-spin alignments should be better described as a linear scaling with the density correlation function on sufficiently large scales.

Inspired by the work of Hui & Zhang (2002), here we suggest a new formula to model

the halo spin-spin correlations:

$$\eta(r) \approx \frac{a_1^2 \xi^2(r; R)}{6 \xi^2(0; R)} + \varepsilon_{\text{nl}} \frac{\xi(r; R)}{\xi(0; R)}, \quad (8)$$

where a nonlinear correlation parameter ε_{nl} is introduced to measure the strength of the nonlinear tidal effect on the halo spin-spin correlations. In this model the linear correlation parameter is notated as a_1 since its value could be different between the two cases that the nonlinear effect is ignored as in equation (4) and taken into account as in (8).

Equation (8) implies that if the nonlinear contribution exists, then the halo spin-spin correlations must exist on larger scale than predicted by the linear model (eq.[4]) since it scales linearly with the density correlation function in the nonlinear model. That is, the nonlinear tidal effect would generate large-scale correlations of the halo spin axes. Of course, the values of the nonlinear correlation parameter ε_{nl} as well as the linear correlation parameter have to be determined empirically.

The cross-correlation, $\eta_C(r)$ can be also modeled in accordance with (8) as

$$\eta_C(r) \approx \frac{a_1^2 \xi_C^2(r; R_1, R_2)}{6 \xi_C^2(0; R_1, R_2)} + \varepsilon_{\text{nl}} \frac{\xi_C(r; R_1, R_2)}{\xi_C(0; R_1, R_2)}. \quad (9)$$

It is worth mentioning that the value of ε_{nl} for the cross correlation $\eta_C(r)$ would not be necessarily lower than its value for the auto-correlation $\eta(r)$ in equation (8), unlike the case of the linear tidal torque model in §2.2. In the nonlinear regime where the non-Gaussianity in the density field grows, the occurrence of the halo merging is quite frequent. This occurrence of the halo merging plays a role of transferring the orbital angular momentum generated by the external tidal field into the spin angular momentum of a merged halo. In other words, the orbital angular momentum of a system composed of small individual halos become the spin angular momentum of a large halo formed through merging of the small halos. Given that the orbital angular momentum of the system before merging is generated by the external tidal field on larger scale (Vitvitska et. al. 2002), the transfer of the orbital angular momentum into the spin angular momentum creates cross-correlations of the tidal fields between different scales, which in turn generates large-scale cross-correlations η_C in the nonlinear regime.

3. SIGNALS FROM NUMERICAL SIMULATIONS

3.1. Numerical Data

We use the halo catalogs from the Millennium Run Simulation ¹ of 10^{10} dark matter particles for a Λ CDM universe with the cosmological parameters given as $\Omega_m = 0.25$, $h = 0.73$, $\sigma_8 = 0.9$ and $n_s = 1$ (Springel et al. 2005). The simulation was performed in a periodic box of linear size of $500h^{-1}\text{Mpc}$ to follow the evolution of all particles from $z = 200$ to $z = 0$, each of which has a mass of $8.6 \times 10^8 h^{-1} M_\odot$.

We analyze the halo catalogs at four different redshifts $z = 0, 0.5, 1$ and 2 which contain information on the halo mass, comoving position, comoving peculiar velocity and the spin vector. At each redshift, we restrict our attention only to those halos which have more than 200 particles for better accuracy in the measurement of the halo spin vector. It amounts to selecting only halos which are more massive than $17.2 \times 10^9 h^{-1} M_\odot$.

Basically, we measure the spatial correlations of the spin axes between neighbor halos as a function of separation distance and investigate how the correlation strength changes with redshift (z), halo mass (M), velocity (v) and specific angular momentum (l , angular momentum per mass). Then, we compare the numerical results with the linear and the nonlinear analytic models described in §2 to determine the best-fit values of the correlation parameters, a , a_l , and ε_{nl} .

3.2. Dependence on the Redshift

Figure 1 plots the halo spin-spin correlation function $\eta(r)$ at $z = 0, 0.5, 1$ and 2 in the top-left, top-right, bottom-left, and bottom-right panel, respectively. In each panel, the solid dots correspond to the numerical results from the Millennium data while the solid and the dashed lines represent the nonlinear model (eq.[8]) and the linear model (eq.[4]), respectively. The case of no alignment is also shown as a dotted line in each panel for comparison.

The errors of the numerical results are calculated as one standard deviation for the case of no alignment. Basically, it is computed by the formula of $2/\sqrt{45n_h}$ where n_h is the number of halos belonging to each bin (Lee & Pen 2001). Note that the sizes of the vertical errors in Figure 1 depend on the value of n_h which in turn depends on the bin size of the spatial separation r . Here we choose the bin size of r as $2h^{-1}\text{Mpc}$ for all plots. We have tested

¹It is now available at <http://www.mpa-garching.mpg.de/millennium>

whether or not the final results depend on the bin size of r and confirmed the robustness of the final results.

For the analytic models, the correlation parameters are determined through fitting to the numerical results by means of the χ^2 -minimization. For the evaluation of the analytic models, we use the formula for the linear power spectrum given by Bardeen et al. (1986) using the same values of the cosmological parameters that are used for the Millennium Run simulations and the shape parameter $\Gamma = \Omega_m h$ (private communication with V. Springel).

Table 1 lists the number of halos (N_h), the mean mass (\bar{M}), the best-fit values of a , a_{nl} and ε_{nl} at $z = 0 - 2$. Here, the mean mass \bar{M} for each bin is used to find the Lagrangian smoothing scale, R which has to be implemented into the analytic models (eqs.4 -8). As shown in Figure 1, we detect clear signals of the halo spin-spin alignments within a few $h^{-1}\text{Mpc}$ distances at all four redshifts. Note, however, a conspicuous difference between the results at low redshifts ($z = 0$ and 0.5) and at higher redshifts ($z = 1$ and 2). At $z = 1$ and 2 , the correlation signals rapidly decrease with distance and disappear at distances around $10h^{-1}\text{Mpc}$. Thus, for the low redshifts, the linear model (dashed line) for itself fits the numerical data pretty well. Whereas, at $z = 0$ and 0.5 the correlation signals decrease rather slowly, still existent to a nonnegligible level at large separations beyond $10h^{-1}\text{Mpc}$. Thus, at low redshifts the nonlinear model (solid line) fits the numerical data much better than the linear model, predicting the existence of the large-scale correlations.

This phenomena can be quantified in terms of the bestfit-values of the correlation parameters listed in Table 1. At $z = 2$, the best-fit value of ε_{nl} is effectively zero within one standard deviation (σ) while the best-fit value of a_1 is higher than 10σ (not marginalized level). In contrast, at $z = 0$ the value of ε_{nl} deviates from zero as significantly as 12σ while the value of a_1 decreases significantly to a 3σ level. It is, however, worth mentioning here that the standard deviation, σ , here is not marginalized. Figure 2 plots the 68%, 95% and 99% contours for a_1 and ε_{nl} at $z = 0 - 2$, showing the degeneracy in putting the constraints on the two parameters. As can be seen, at $z = 0$ and 0.5 , the values of ε_{nl} deviate from zero at higher than 99% level.

Our numerical detection implies that the linear model for the halo spin-spin correlations (eq.[4]) works well at $z > 1$ but the nonlinear effect indeed dominates at low redshifts ($z < 1$), producing large-scale correlations of the halo spins, which can be well described by our nonlinear model (eq.[8]).

3.3. Dependence on the Specific Angular Momentum Magnitude

We define the magnitude of the rescaled specific angular momentum (angular momentum per unit mass) as $l \equiv L/M_*$ where L and M_* are the halo angular momentum magnitude and the halo mass in unit of $10^{10}h^{-1}M_\odot$, respectively. To determine quantitatively how the halo spin-spin correlation changes with l , we classify the halos at $z = 0$ into four logarithmic bins of l and measure the correlations separately for each bin. Figure 3 plots $\eta(r)$ at four logarithmic bins of l in the top-left, top-right, bottom-left, and bottom-right panels, respectively. Table 2 also lists the number of halos, the mean mass, the best-fit values of a , a_1 and ε_{nl} for each bin, and Figure 4 plots the 68%, 95% and 99% contours for a_1 and ε_{nl} at the four bins.

As shown in Figure 3, in the bins of low- l halos (top two panels), the correlations are rather weak and rapidly diminish to zero at separations greater than a few $h^{-1}\text{Mpc}$. Thus, for this case the linear model with the single parameter a fits the data pretty well. In other words, for the spin-spin correlations of low- l halos, the values of ε_{nl} are effectively zero as shown in Table 2. While in the bins of high- l halos, the correlations are stronger, still existent even at separations as large as $10h^{-1}\text{Mpc}$. Therefore for the spin-spin correlations of high- l halos, the nonlinear model with non-zero value of ε_{nl} fits the data much better than the linear model. Note that for the case of highest- l halos, the value of ε_{nl} is approximately 0.005, which is five times greater than the average value of 0.001 at $z = 0$.

This phenomena that the halos with higher specific angular momentum tend to have stronger non-linear (and linear) spin-spin correlations may be explained as follows. If a halo is located in a region where the effect of the tidal field is very strong, then the halo will possess high specific angular momentum. Furthermore, its spin direction will be strongly correlated with that of its neighbors since the strong effect of the tidal field tends to diminish any randomization of the spin orientations that can occur in the subsequent stages. Therefore, those halos which have higher specific angular momentum are likely to show strong spin-spin correlations under the strong effect of the tidal field. We have also explored whether this phenomena occur at higher redshifts $z = 0.5, 1$ and 2 and found that this is still the case.

3.4. Dependence on the Mass Scale

The halos at $z = 0$ are classified into four bins according to the value of the rescaled mass M_* and their spin-spin alignments are measured separately for each bin. Figure 5 plots $\eta(r)$, Table 3 lists the number of halos, the mean mass, the best-fit values of a , a_1 and ε_{nl} , and Figure 2 plots the 68%, 95% and 99% contours for a_1 and ε_{nl} for the four bins.

As shown in Figure 5, in the third bin which includes the galactic halos with mass of

order of $(1 - 2) \times 10^{12} h^{-1} M_{\odot}$ (bottom-left panel), the correlation signal is strongest, existent at separations as large as $10 h^{-1} \text{Mpc}$. For this bin, the nonlinear model with nonzero value of ε_{nl} gives a better fit the numerical results than the linear with model single parameter a . The best-fit value of ε_{nl} deviates from zero by a factor of 3σ as shown in Table 3. Whereas in the first and the fourth bins which include dwarf halos and galaxy-group halos, respectively, the signals are rather weak and the correlations disappear at large distances. For these bins, the linear model for itself fits the numerical data quite well and the values of ε_{nl} are effectively zero. This result implies that the strength of the nonlinear effect depends on mass scales, being strongest on the galactic mass scale. Note, however, here that the value of the characteristic mass scale changes with z . Thus, the results given in §3.2 and §3.4 are related to each other.

3.5. Scale Bias and Cross-Correlations

As mentioned in §2.3, if the nonlinear effect dominates on the halo spin-spin correlations, then it is likely to produce stronger cross-correlations between different mass scales (eq.[9]). We measure the halo spin cross-correlations between the halos of different mass bins that are constructed in §3.2 (the first bin corresponds to the lowest mass scales. see Table 3), and find the best-fit values of a , a_{nl} and ε_{nl} by fitting the numerical data to the analytic model (eq.[9]).

Figure 7 plots the numerical results of η_C for the six different cases: η_{C12} , η_{C13} , η_{C14} , η_{C23} , η_{C24} , η_{C34} , where η_{Cij} represents the cross-correlations between the i -th and the j -th mass bins. As can be seen, the nonlinear model basically gives better fit to the numerical result for all cases, indicating that the nonlinear effect increases indeed increase spin cross-correlations between different mass scales, as presumed in §2.3. Figure 9 plots the 68%, 95% and 99% contours for a_1 and ε_{nl} for these two cases of η_{13} and η_{23} where the strong signals of the cross-correlations are detected. Obviously, the values of ε_{nl} for each case deviates from zero at 95% confidence level.

3.6. Dependence on the Velocity Magnitude

We also investigate the dependence of the halo spin-spin correlations on the magnitude of halo peculiar velocity v in unit of km/s. The correlations $\eta(r)$ are plotted in Fig.10 at four logarithmic bins of v , and the 68%, 95% and 99% contours for the correlation parameters of the nonlinear models are shown in Fig.11.

As shown in Figure 10, the dependence of the halo spin-spin correlations on the velocity magnitude turns out not to be so strong. The significant nonlinear effect on the halo-halo correlation is found only in the first bin of low- v halos (top-left panel), For this bin, the linear model fails in fitting the numerical data while the nonlinear model gives a better fit, predicting the large-scale correlations. As shown in the top-left panel of Fig.11, the value of ε_{nl} for the case of lowest- v halos deviates from zero at 95% confidence level.

4. SUMMARY AND DISCUSSION

We summarize our results in the following:

- To account for the possible nonlinear tidal effect on the intrinsic halo alignments, we suggest a new model characterized by two free parameters, a_1 and ε_{nl} . The two parameters a_1 and ε_{nl} represents the strength of the linear and the nonlinear tidal effect on the orientations of the halo spins, respectively. If $\varepsilon_{\text{nl}} = 0$, it corresponds to the case that the nonlinear tidal effect is negligible and the halo spin-spin correlations is a quadratic scaling of the density correlation function $\xi(r)$, existent on small scales. While if ε_{nl} deviates from zero, the nonlinear tidal effect is nennegligible and the halo spin-spin correlations is a linear scaling of $\xi(r)$, present on large distance scales.
- Using the halo catalogs from numerical simulations at $z = 0, 1, 0.5$ and 2 , we have measured the halo spin-spin correlations and determined the best-fit values of a_1 and ε_{nl} . It is found that the values of a_1 increases with z while ε_{nl} decreases with z . At $z = 1$ and 2 , the values of ε_{nl} are found to be negligibly small, while at $z = 0.5$ and $z = 0$ ε_{nl} has an order of 10^{-3} higher than 5σ . Especially at $z = 0$, a_1 is effectively zero and ε_{nl} deviates from zero by a factor more than 10σ , which implies that at present epoch the nonlinear tidal effect is dominant inducing halo spin correlations on scales as large as $10h^{-1}\text{Mpc}$.
- We have investigated the dependence of a_1 and ε_{nl} on the halo intrinsic properties such as mass (M), specific angular momentum magnitude (l), and velocity magnitude (v) at $z = 0$. It is found that the value of ε_{nl} depends most sensitively on the value of l . For those halos with highest l , the value of ε_{nl} reaches as high as 5×10^{-3} and the value of a_1 is effectively zero. Regarding the dependence on M and v , it is found that ε_1 is less sensitive. However, for those halos with $M \sim (1 - 2) \times 10^{12}h^{-1}M_{\odot}$ $\log v < 2.5\text{km/s}$, the value of ε_{nl} tend to be higher.
- We have measured the cross-correlations of the spin axes between halos on different mass scales. It is found that on two different galactic mass scales ($M_1 \sim 10^{11}h^{-1}M_{\odot}$

and $M_s \sim 10^{12} h^{-1} M_\odot$, the cross-correlations exist at scales as large as $10 h^{-1} \text{Mpc}$, due to the growth of the non-Gaussianity increases cross-correlations of the tidal field on different scales.

Our results have shown that the galaxy intrinsic alignments can exist not only for the case that the separation distance between the two galaxies is small but also for the case that any galaxy pair separated by distances larger than $10 h^{-1} \text{Mpc}$ can still have aligned axes. It also implies preferential E-mode contamination of the galaxy intrinsic alignments in weak lensing signals (Crittenden et al. 2002).

In addition, we have also found quantitatively that the galaxy intrinsic alignments could be cross-correlated with the larger-scale tidal field. These results imply that the intrinsic galaxy correlations are indeed correlated with the surrounding density field on large scales, which will in turn lead to correlation between the gravitational lensing shears and the intrinsic galaxy alignments, (often called, GI correlations).

Recently, Hirata et al. (2007) claimed that a signal of the GI correlations has been detected from the large low-redshift galaxy surveys (see also, Mandelbaum et al. 2006). According to their claim, the GI correlations exist to a nonnegligible level for the bright Luminous Red Galaxies (LRGs) and it is zero for the faint blue galaxies, mentioning an uncertainty in the estimation of the GI correlation for the faint blue galaxies. According to our numerical detection, the nonlinear tidal effect which causes the large-scale intrinsic alignments is strongest for the halos with high specific angular momentum magnitude and low peculiar velocity, which usually correspond to the galaxies with low surface brightness (Jimenez et al 1998, and references therein) and blue color (Davis et al. 1997). Thus, our results indicate that the GI correlation amplitude for the faint blue galaxies, may exceed the estimation upper limit, as noted by Hirata et al. (2007). It will be of interest to compare the cross-correlations between the spin axes of the blue galaxies and the shapes of the red galaxies for the comparison of their correlation scales.

The Millennium Run simulation used in this paper was carried out by the Virgo Supercomputing Consortium at the Computing Centre of the Max-Planck Society in Garching. We thank V. Springel and G. Lemson for useful comments. We also thank an anonymous referee for helpful suggestions. J.L. is very grateful to the warm hospitality of L. Kofman and the Canadian Institute for Theoretical Astrophysics (CITA) where this work was initiated and performed. J.L. acknowledges the financial support from the Korea Science and Engineering Foundation (KOSEF) grant funded by the Korean Government (MOST, NO. R01-2007-000-10246-0).

REFERENCES

- Aragon-Calvo, M. A., van de Weygaert, R., Jones, B. J. T., & van der Hulst, J. M. 2007, *ApJ*, 655, 5
- Bardeen, J. M., Bond, J. R., Kaiser, N., & Szalay, A. S. 1986, *ApJ*, 304, 15
- Bond, J., R., Kofman, L., & Pogosyan, D. 1996, *Nature*, 380, 603
- Brown, M. L., Taylor, A. N., Hambly, N. C., & Dye, S. 2002, *MNRAS*, 333, 501
- Catelan, P., Kamionkowski, M., & Blandford, R. D. 2001, *MNRAS*, 320, L7
- Catelan, P., & Theuns, T. 1996, *MNRAS*, 282, 436
- Crittenden, R. G., Natarajan, P., Pen, U. L & Theuns, T. 2001, *ApJ*, 559, 552
- Crittenden, R. G., Natarajan, P., Pen, U. L & Theuns, T. 2001, *ApJ*, 568, 20
- Croft, R. A. C. & Metzler, C. A. 2000, *ApJ*, 545, 561
- Davis, M., Miller, A., & White, S.D.M. 1997, *ApJ*, 490, 63
- Doroshkevich, A. G. 1970, *Astrofizika*, 6, 581
- Hahn, O., Porciani, C., Carollo, C. M., & Dekel, A. 2007, *MNRAS*, 375, 489
- Heavens, A., Refregier, A., & Heymans, C. 2000, *MNRAS*, 319, 649
- Heymans, C. & Heavens, A. 2003, *MNRAS*, 339, 711
- Heymans, C., Brown, M., Heavens, A., Meisenheimer, K., Taylor, A., & Wolf, C. 2004, *MNRAS*, 361, 160
- Hirata, C. M. & Seljak, U. 2004, *Phys. Rev. D*, 70, 063526
- Hirata, C. M., et al. 2004, *MNRAS*, 353, 529
- Hirata, C. M., et al. 2007, *MNRAS*, 381, 1197
- Hui, L. & Zhang Z. 2002, preprint [astro-ph/0205512]
- Jimenez, R., Padoan, P., Matteucci, F. & Heavens, A. F. 1998, *MNRAS*, 299, 123
- Jing, Y. 2002, *MNRAS*, 335, L89
- King, L. 2005, *A&A*, 441, 47

- Lee, J., Kang, X., & Jing, Y. 2005, ApJ, 629, L5
- Lee, J. & Pen, U. L. 2000, ApJ, 532, L5
- Lee, J. & Pen, U. L. 2001, ApJ, 555, 106
- Lee, J. & Pen, U. L. 2002, ApJ, 567, 111
- Lee, J. & Erdogdu, P. 2007, 671, 1248
- Mandelbaum, R., Hirata, C. M., Ishak, M., Seljak, U., & Brinkmann, J. 2006, MNRAS, 367, 611
- Mo, H. J., Mao, S. & White, S. D. M. 1998, MNRAS, 295, 319
- Navarro, J.F., Abadi, M.G., & Steinmetz, M. 2004, ApJ, 613, L41
- Patiri, S. G., Cuesta, A. J., Prada, F., Betancort-Rijo, J., & Klypin, A. 2006, ApJ, 652, 75
- Peebles, P. J. E. 1969, ApJ, 155, 393
- Pen, U. L., Lee, J., & Seljak, U. 2000, 543, L107
- Porciani, C., Dekel, A., & Hoffman, Y. 2002, MNRAS, 332, 339
- Springel, V. et al. 2005, Nature, 435, 629
- Takada, M., & White, S. D. M. 2004, ApJ, 601, L1
- Trujillo, I., Carretero, C., & Patiri, S. 2006, ApJ, 610, L111
- Vitvitska, M., Klypin, A. A., Kravtsov, A. V., Wechsler, R. H., Primack, J. R., & Bullock, J. S. 2002, ApJ, 581, 799
- White, S. D. M. 1984, ApJ, 286, 38

Table 1. The number of halos, the mean mass, the best-fit values of the linear and the nonlinear correlations parameters for the intrinsic halo spin correlations at four redshifts from the Millennium Run data.

z	N_h	\bar{M}_* ($10^{10}h^{-1}M_\odot$)	$a \times 10^2$	$a_1 \times 10^2$	$\varepsilon_{\text{nl}} \times 10^3$
0	1846776	169.7	11.3 ± 0.6	3.9 ± 1.6	1.2 ± 0.1
0.5	1942263	133.3	9.8 ± 0.7	6.1 ± 1.1	0.7 ± 0.1
1	1928690	106.7	8.6 ± 0.8	7.9 ± 0.9	0.1 ± 0.1
2	1558504	69.6	10.6 ± 0.9	10.4 ± 0.9	0.0 ± 0.2

Table 2. Numerical results for the intrinsic halo spin correlations at four bins of the specific angular momentum magnitude l .

$\log(l)$	N_h	\bar{M}_* ($10^{10}h^{-1}M_\odot$)	$a \times 10^2$	$a_1 \times 10^2$	$\varepsilon_{\text{nl}} \times 10^3$
(−4.0, −2.0)	350541	607.1	9.4 ± 2.4	9.4 ± 2.4	0.0 ± 0.4
(−2.0, −1.7)	604356	102.7	10.1 ± 2.2	6.6 ± 3.4	0.7 ± 0.4
(−1.7, −1.5)	475842	51.0	16.8 ± 2.1	5.4 ± 6.3	2.7 ± 0.6
(−1.5, 0.0)	416032	32.5	20.2 ± 2.2	0.0 ± 9.7	4.9 ± 0.8

Table 3. Numerical results for the intrinsic halo spin correlations at four different mass ranges.

M_* ($10^{10}h^{-1}M_\odot$)	N_h	\bar{M}_* ($10^{10}h^{-1}M_\odot$)	$a \times 10^2$	$a_1 \times 10^2$	$\varepsilon_{\text{nl}} \times 10^3$
(17.2, 38.0)	925011	25.0	14.1 ± 1.6	8.5 ± 2.6	1.3 ± 0.4
(38.0, 85.0)	469647	55.7	14.1 ± 2.3	10.6 ± 3.2	1.0 ± 0.6
(85.0, 190.0)	233724	124.6	20.8 ± 2.5	15.0 ± 3.5	2.4 ± 0.9
(190.0, 10^5)	218248	1022.5	15.5 ± 1.9	13.0 ± 2.2	0.8 ± 0.6

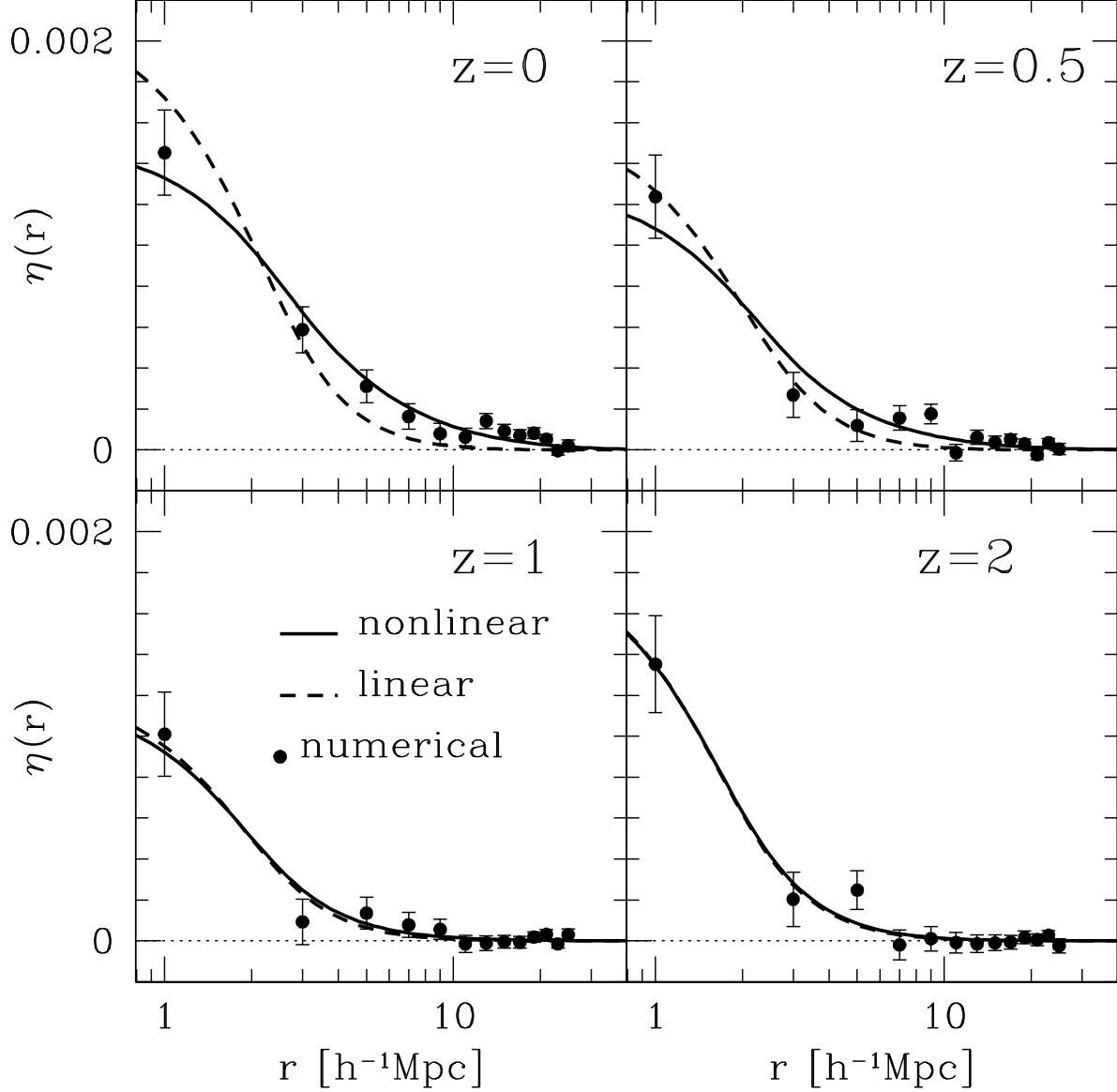


Fig. 1.— Intrinsic halo spin-spin correlations at four different redshifts: $z = 0, 0.5, 1$ and 2 (top-left, top-right, bottom-left, and bottom-right, respectively). In each panel, the solid dots represent the numerical results, while the solid and dashed lines correspond to the nonlinear (eq.[4]) and linear (eq.[4]) analytic model, respectively. The errors are calculated as the standard deviation for the case of no correlation. The dotted line represents the case of no correlation.

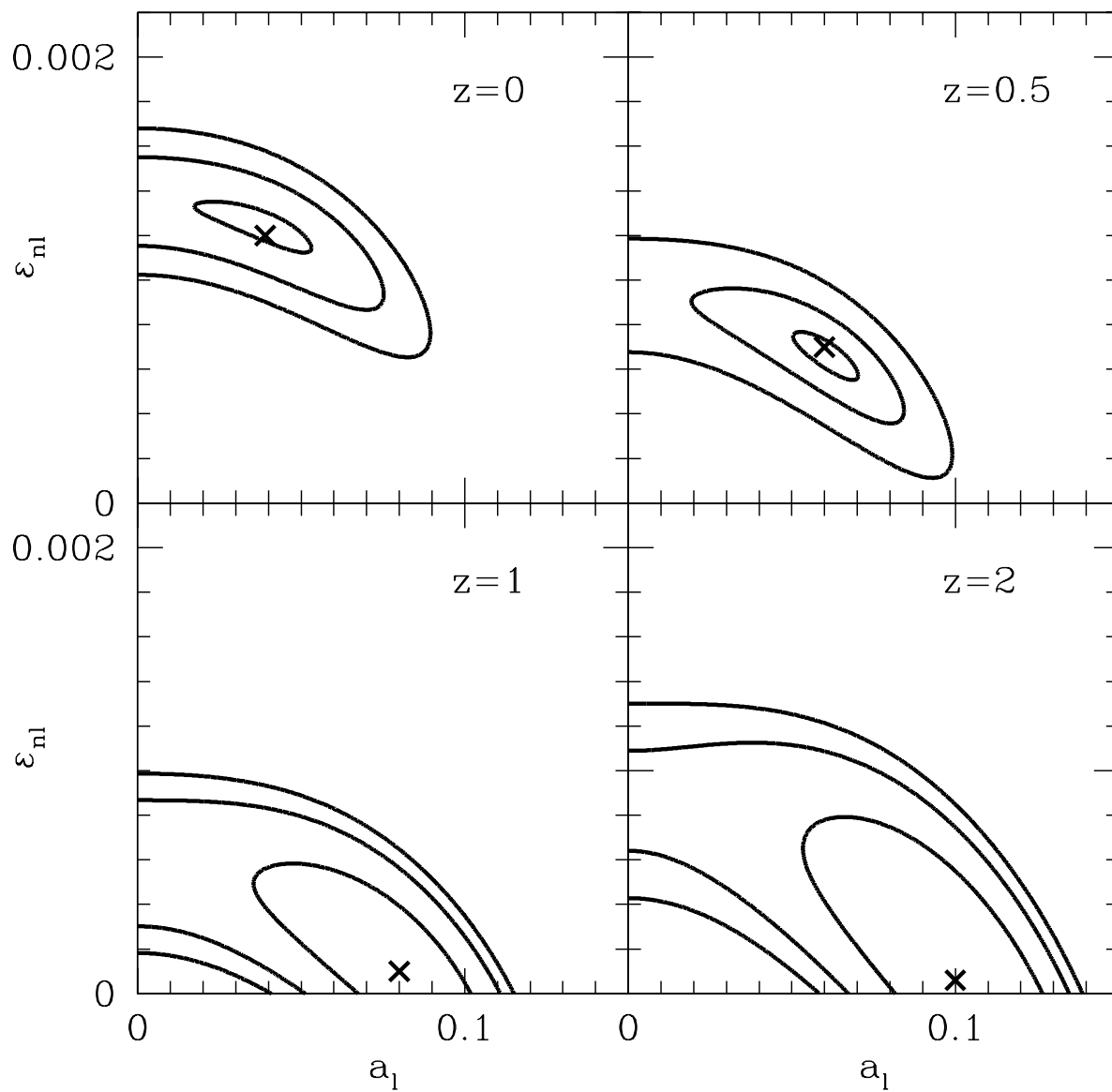


Fig. 2.— 68%, 95% and 99% contour plots for the linear and the nonlinear correlation parameters, a_1 and ε_{nl} at $z = 0, 0.5, 1$ and 2 (top-left, top-right, bottom-left, and bottom-right, respectively). In each panel, the cross mark represents the best-fit value.

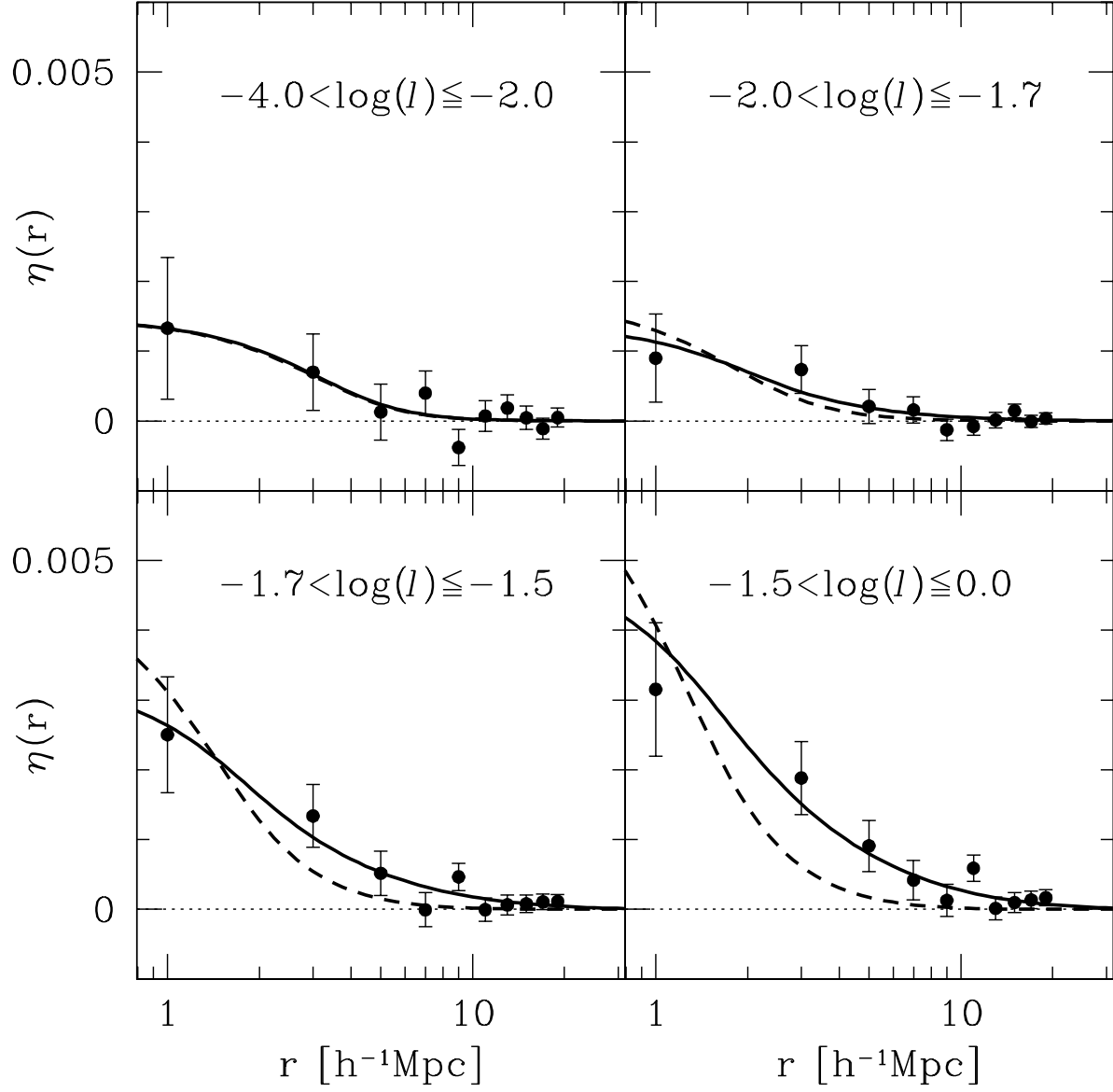


Fig. 3.— Intrinsic halo spin-spin correlations at $z = 0$ for the four different logarithmic bins of the specific angular momentum magnitude l at $z = 0$.

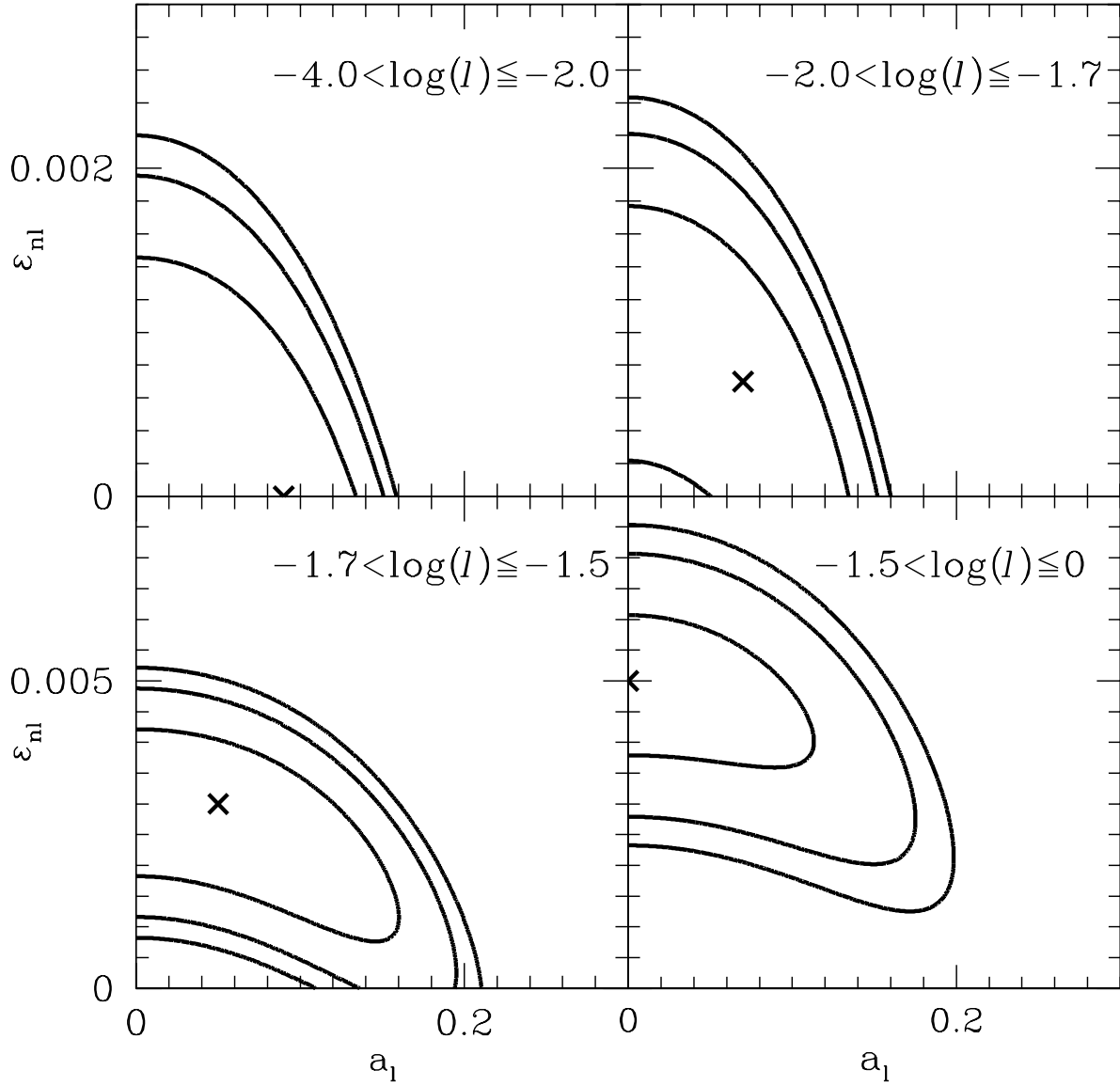


Fig. 4.— 68%, 95% and 99% contour plots for a_1 and ε_{nl} at the four logarithmic bins of l .

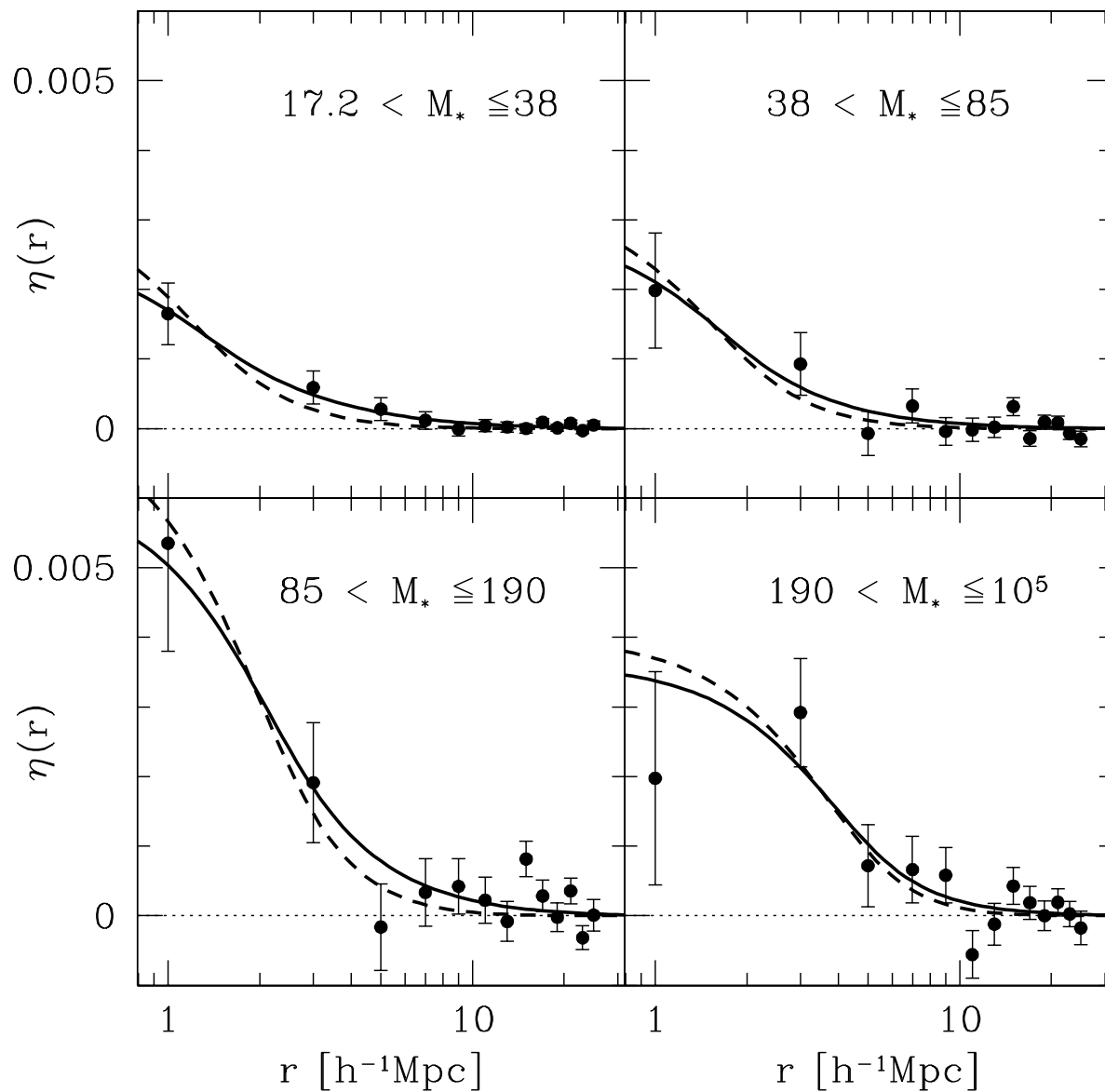


Fig. 5.— The dark halo spin-spin correlations at $z = 0$ for the four different bins of the halo mass M_* in unit of $10^{10}h^{-1}M_\odot$.

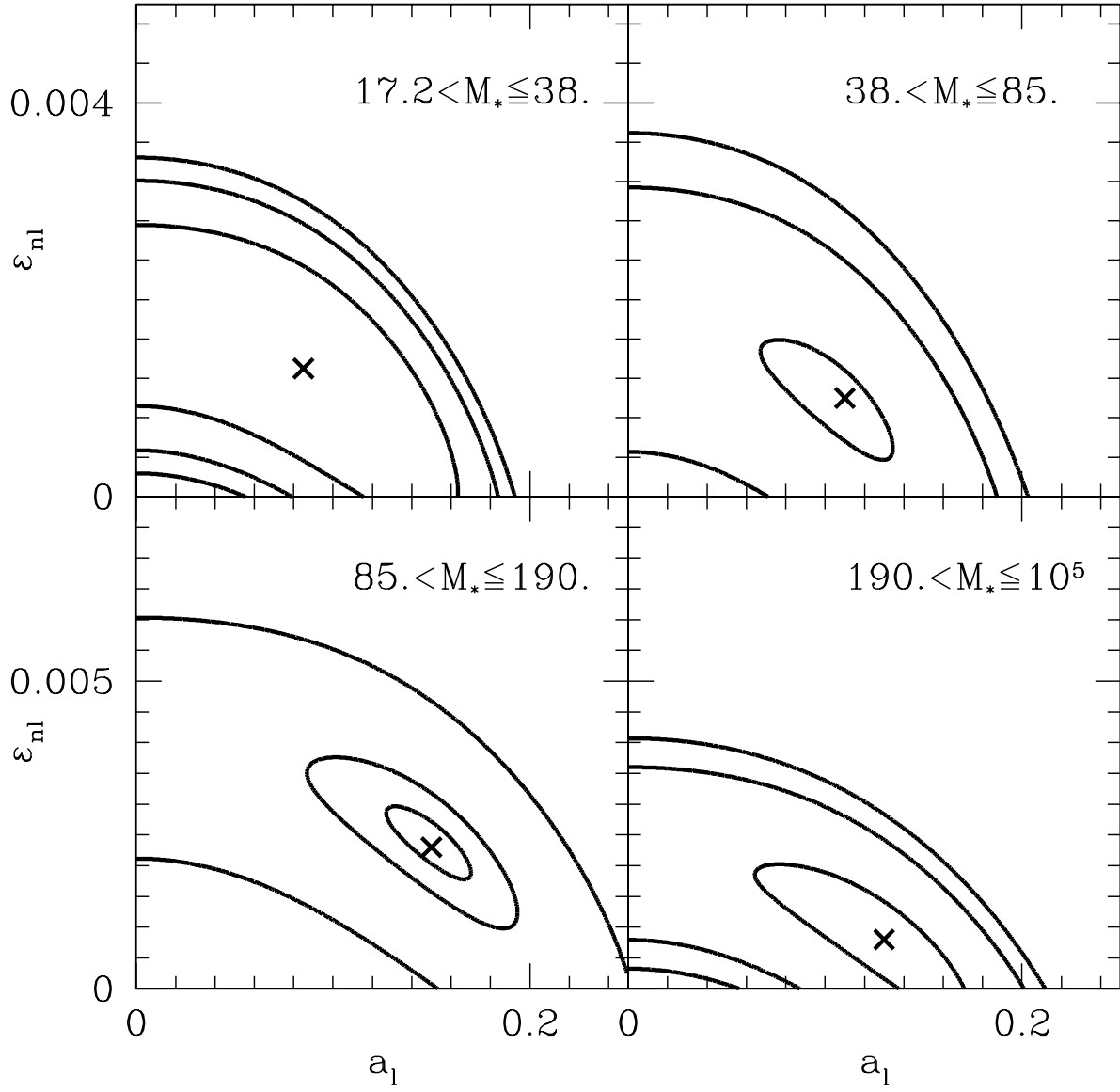


Fig. 6.— 68%, 95% and 99% contour plots for a_1 and ε_{nl} at the four bins of halo mass M_* .

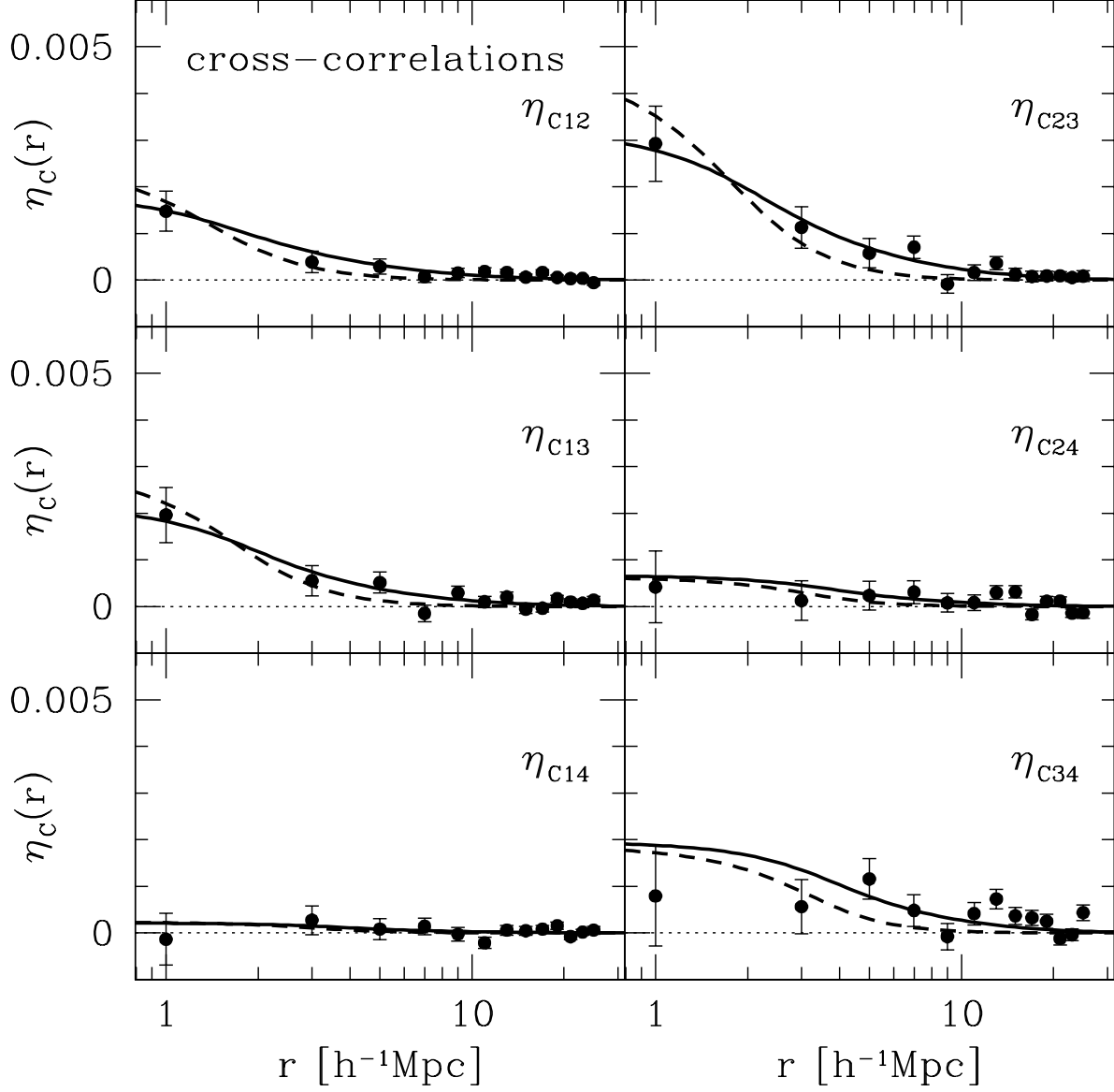


Fig. 7.— Intrinsic halo spin cross correlations between different mass scales at $z = 0$. In each panel, η_{Cij} represents the cross-correlation between the i -th and the j -th mass bin, given in Table 3.

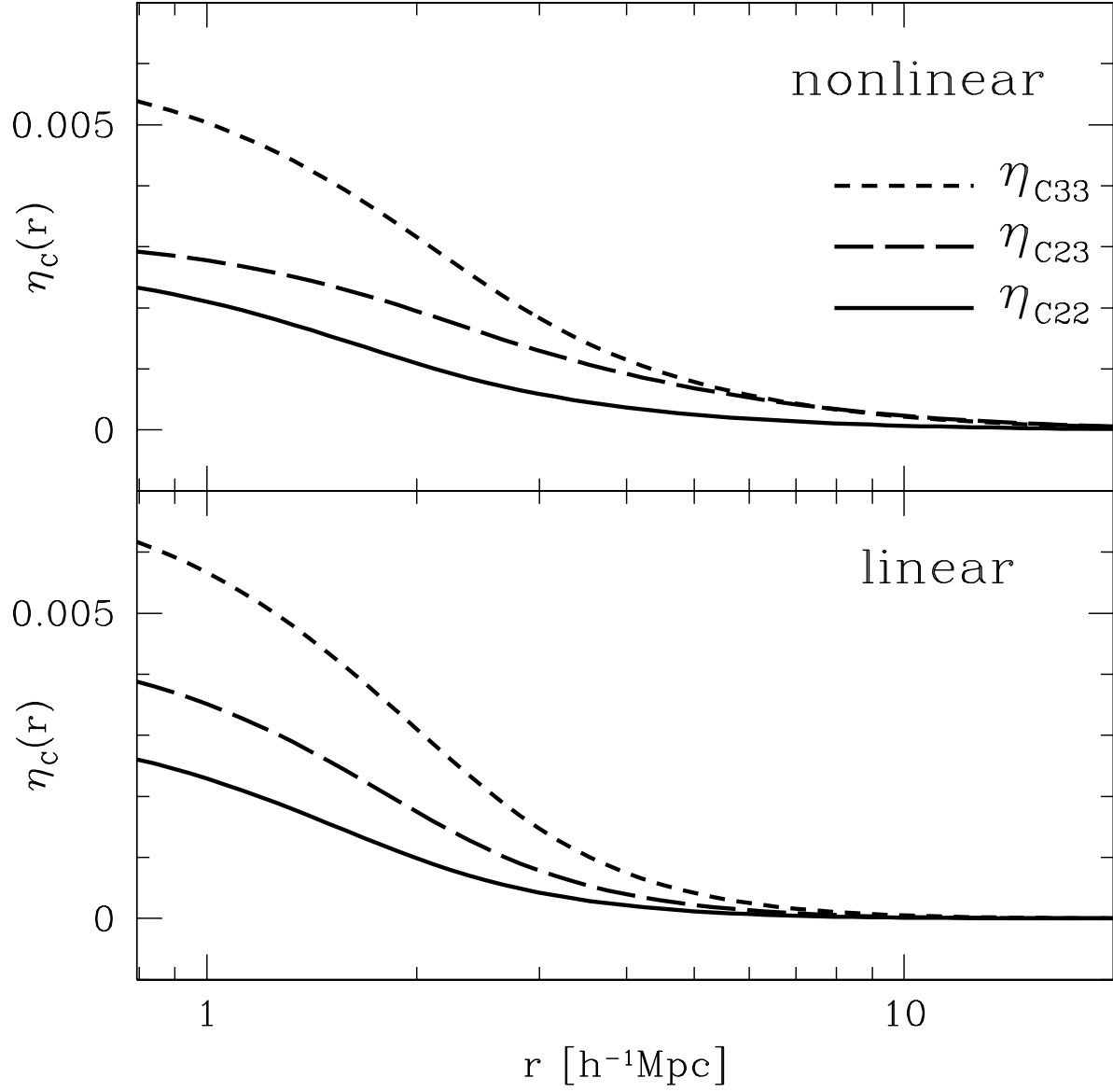


Fig. 8.— Comparison of the spin correlation $\eta_{ii}(r)$ between halos in the same mass bins with the spin cross-correlation $\eta_{Cij}(r)$ between halos in different mass bins.

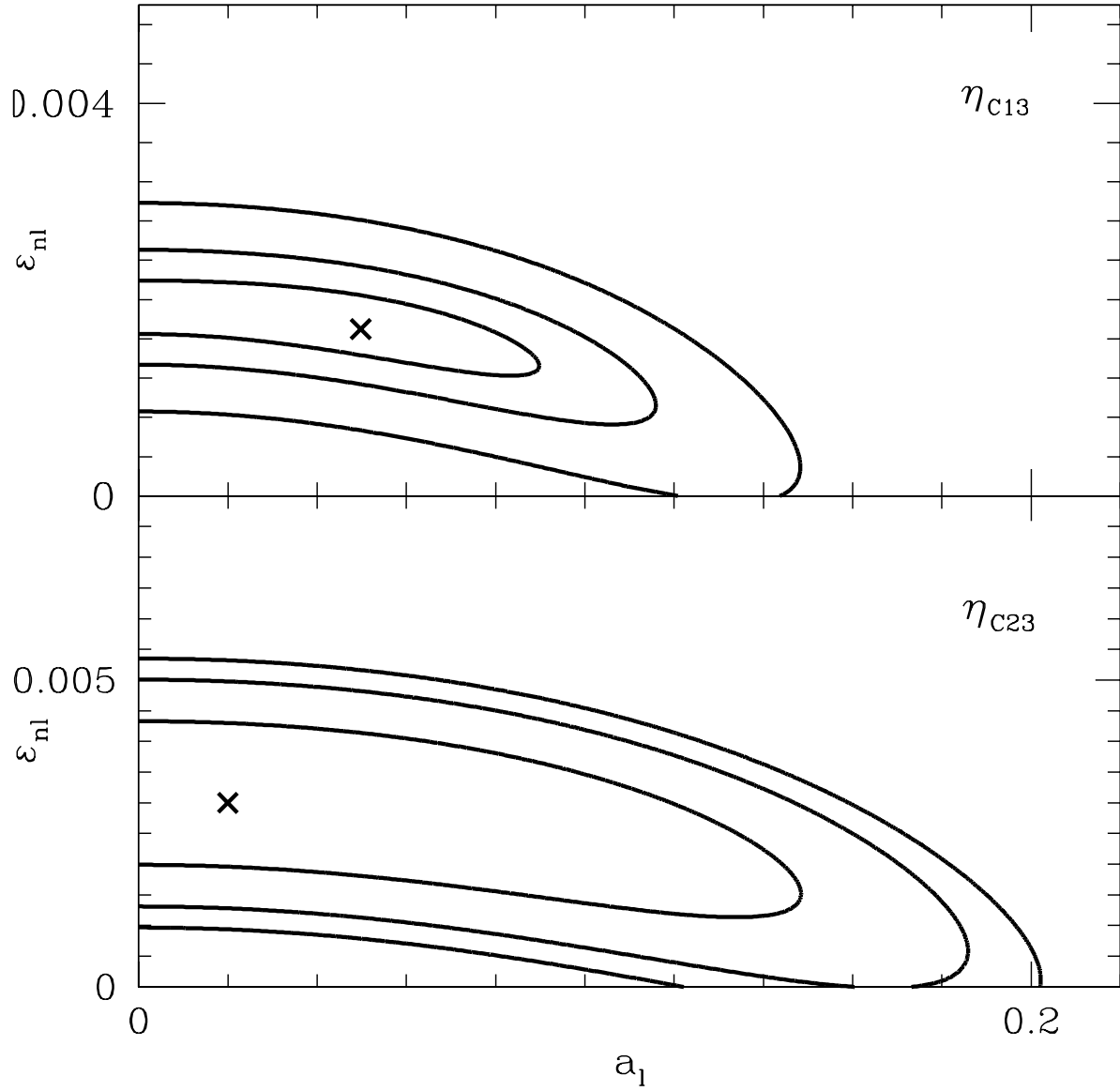


Fig. 9.— 68%, 95% and 99% contour plots for a_1 and ϵ_{nl} for the spin cross-correlations between halos in the 1st mass bin and the 2nd mass bin (top) and between halos in the 2nd mass bin and the 3rd mass bin (bottom).

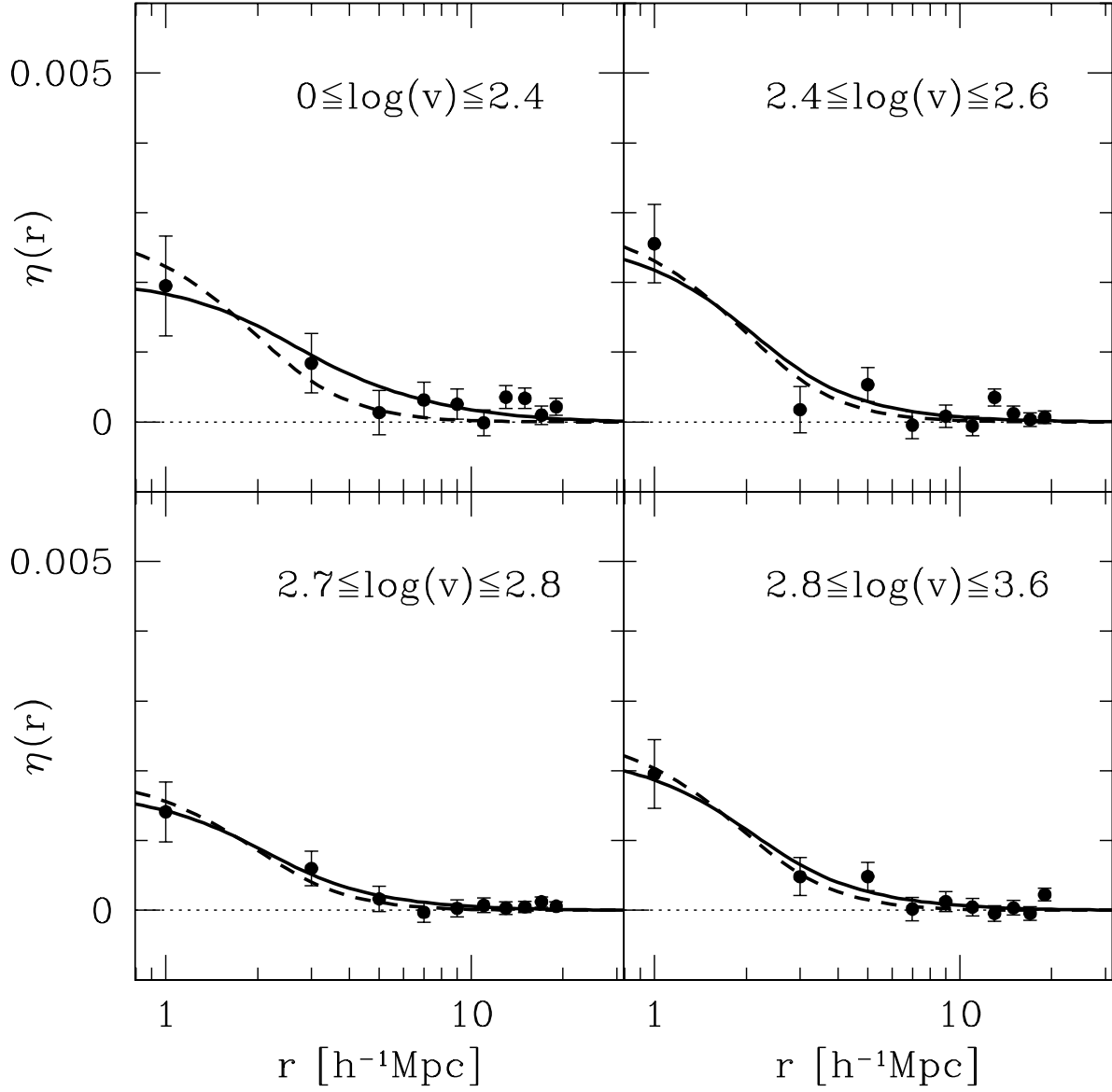


Fig. 10.— Intrinsic halo spin correlations at the four logarithmic bins of the velocity magnitude v in unit of km/s.

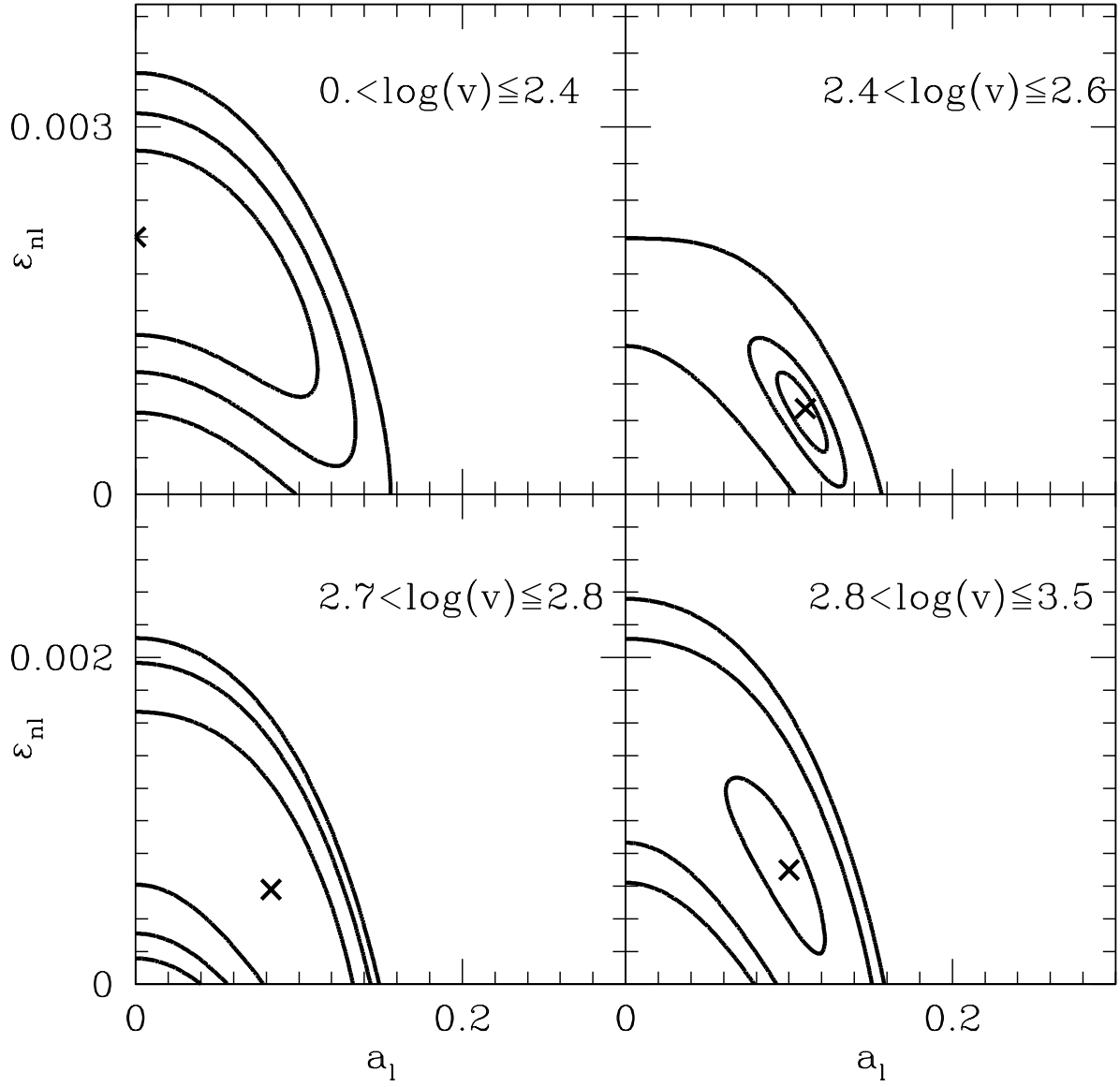


Fig. 11.— 68%, 95% and 99% contour plots for a_1 and ϵ_{nl} at the four logarithmic bins of v .